

# Star Formation Histories of Nearby Elliptical Galaxies. II. Merger Remnant Sample

Justin H. Howell

*UCO/Lick Observatory, Department of Astronomy & Astrophysics,  
University of California, Santa Cruz, California 95064, USA  
jhhowell@ucolick.org<sup>1</sup>*

## ABSTRACT

This work presents high  $S/N$  spectroscopic observations of a sample of six suspected merger remnants, selected primarily on the basis of HI tidal debris detections. Single stellar population analysis of these galaxies indicates that their ages, metallicities, and  $\alpha$ -enhancement ratios are consistent with those of a representative sample of nearby elliptical galaxies. The expected stellar population of a recent merger remnant, young age combined with low  $[\alpha/\text{Fe}]$ , is not seen in any HI-selected galaxy. However, one galaxy (NGC 2534), is found to deviate from the  $Z$ -plane in the sense expected for a merger remnant. Another galaxy (NGC 7332), selected by other criteria, best matches the merger remnant expectations.

*Subject headings:* galaxies: elliptical and lenticular, cD — galaxies: abundances — galaxies: stellar content — galaxies: formation — galaxies: evolution — galaxies: interactions — galaxies: general

## 1. Introduction

The formation mechanisms for early-type galaxies have been the subject of intense scrutiny over the past several decades. The early dynamical simulations of Toomre & Toomre (1972) showed that merger events between two spiral galaxies can result in an elliptical galaxy as the merger remnant. This provides a striking alternative to the classical monolithic collapse picture of elliptical galaxy formation (e. g. Larson 1974), in which the entire galaxy forms in a single star-formation event at high redshift. Although mergers in progress are obvious, merger remnants evolving into elliptical galaxies are more difficult to identify. Such objects populate the “King gap” (King 1977) separating interacting galaxies from the quiescent elliptical remnant galaxy they are proposed to become. For purposes of this study, major mergers are defined as those encounters in which the mass ratio is

---

<sup>1</sup>now at the Infrared Processing and Analysis Center, Mail Stop 100-22, California Institute of Technology, Jet Propulsion Laboratory, Pasadena, CA 91125; jhhowell@ipac.caltech.edu

large enough that any stellar disks are disrupted and transformed into an elliptical merger remnant. Minor mergers or accretion events are defined as encounters in which the structure of the higher-mass progenitor (whether elliptical or spiral) is preserved in the remnant.

The predicted stellar populations of merger remnants depend greatly on the gas fraction in the progenitor galaxies. In the extreme case suggested by Ashman & Zepf (1992), where ellipticals form from predominantly gaseous spiral galaxies, the resulting stellar population will differ from that of a monolithic collapse elliptical only in age.

An alternative expectation for the stellar population of the remnant of a recent major merger event is similar to the frosting model of Trager et al. (2000). The starburst at the time of the merger event involves only a small fraction of the total mass of the system, with the bulk of the galaxy being older and less metal-rich. A key difference between the expectations of such a merger remnant and an elliptical formed in a single starburst is that the latter will have high  $[\alpha/\text{Fe}]$  due to the short formation timescale, while stars formed within two spiral galaxies will have near solar  $[\alpha/\text{Fe}]$  (Thomas, Greggio, & Bender 1999). In a merger between spiral galaxies which have already converted much of their mass into stars, the burst population will also have low  $[\alpha/\text{Fe}] \leq 0.1$ , as the gas from which it forms has been enriched with iron from billions of years of SN Ia. Thomas et al. (1999) showed that although it is possible for a merger scenario to produce the high  $[\alpha/\text{Fe}]$  values seen in most early-type galaxies, a flat initial mass function (IMF) for the merger starburst population is required in order to produce sufficient  $\alpha$ -elements. This prediction of low  $[\alpha/\text{Fe}]$  is generalized to any galaxy formed hierarchically by Thomas (1999) using the semianalytic models of Kauffmann (1996). The recent work of Nagashima et al. (2005) arrives at the same conclusions, obtaining enhanced  $[\alpha/\text{Fe}]$  only for a top-heavy IMF, or near solar  $[\alpha/\text{Fe}]$  using an IMF more typical of quiescent star formation in spiral galaxies.

The paper is organized as follows. The sample selection and data are described in § 2. Stellar population analysis is performed in § 3, and conclusions are discussed in § 4.

## 2. Sample Selection and Data

The bulk of the merger remnant sample was selected based on detections of HI tidal debris (J. Hibbard 2000, private communication). As Hibbard & Mihos (1995) showed, gas in tidal tails can remain bound but at large radii for several Gyr after a major merger event. This criterion preferentially selects early-type galaxies resulting from gas-rich encounters. Galaxies which accreted a gas-rich satellite are the primary contaminants for a sample of major merger remnants using this HI selection criterion. For example, van Gorkom et al. (1986) proposed such an accretion event to explain the HI observations of NGC 1052, and van Driel, Balkowski, & van Woerden (1989) made a similar argument about NGC 3619. Other selection criteria, such as the fine structure parameter of Schweizer & Seitzer (1992), are sensitive to all types of merger event, major or minor, gas-rich or gas-poor. Hibbard & Sansom (2003) have shown that galaxies with large fine structure parameters

are no more likely than those with little fine structure to have associated HI tidal debris. One galaxy in the selected sample, NGC 1052, is also a member of the volume-limited sample of Howell (2005, hereafter Paper I) The merger remnant sample is listed in Table 1. Morphological T-types (de Vaucouleurs et al. 1995) and the  $S/N$  ratio per pixel near the  $H\beta$  line are listed for each galaxy.

NGC 7332 does not satisfy the HI selection criterion (Burstein, Krumm, & Salpeter 1987) but shows other indications suggesting a merger origin. Deviations from the Fundamental Plane (Prugniel & Simien 1996; Forbes, Ponman, & Brown 1998) suggest a young age, and Schweizer & Seitzer (1992) find substantial fine structure ( $\Sigma = 4.00$ ) and a young heuristic merger age  $\sim 5$  Gyr. Although NGC 7332 has a bimodal color distribution of globular clusters, the age of the red population has not been spectroscopically determined. The galaxy itself has been studied spectroscopically; see Terlevich & Forbes (2002) for a summary. The SAURON group has recently observed the entire galaxy at a limited wavelength coverage (Falc3n-Barroso et al. 2004). Both spectroscopic studies find consistent ages of 4.5–5 Gyr.

Optical images overlaid with HI maps are presented for five galaxies in the merger remnant sample in Figs. 1–5. NGC 474 is a gas-poor shell galaxy interacting with the nearby gas-rich spiral galaxy NGC 470. It has a very large fine structure index  $\Sigma = 5.26$  and a relatively young heuristic merger age  $\sim 4$  Gyr (Schweizer & Seitzer 1992). However, the heuristic merger age is based on an analysis of  $UBV$  color information, which is known to be insufficient to break the age-metallicity degeneracy (Worthey 1994). NGC 1052 is a prototypical LINER system (Heckman 1980) with two HI tails (Fig. 2). Schweizer & Seitzer (1992) find little fine structure ( $\Sigma = 1.78$ ) and a heuristic merger age  $\sim 8$  Gyr. NGC 2534 has a single extended HI tail, as shown in Fig. 3. In NGC 3619, the HI emission is colocated with the galaxy’s stellar component, with a smaller characteristic radius (Fig. 4). NGC 5903 shows extended HI both within the galaxy and in two long tidal tails (Fig. 5).

By construction, this sample is expected to have young ages as noted above. Assuming that these galaxies formed in major merger events (and that the merger starburst did not have an IMF strongly biased towards massive stars), they are also expected to have low  $[\alpha/Fe]$  (Thomas et al. 1999).

Observations and data analysis were performed identically as for the volume-limited sample described in Paper I. Longslit spectra were taken using the Kast spectrograph with the 1200 lines/mm grating blazed at  $5000\text{\AA}$  on the Lick 3 meter telescope. The  $145''$ -long slit was oriented along the galaxy’s major axis. Four 25 minute exposures were taken on each galaxy, interspersed with 5 minute sky exposures taken several arcminutes away. The spectral range was  $4200\text{\AA}$ – $5600\text{\AA}$ , with instrumental resolution of approximately 100 km/s. The slit width was typically  $1.5''$ , though in poor seeing conditions this was increased to  $2''$ . The plate scale for the spectrograph in this configuration was  $1.17\text{\AA}/\text{pixel}$  in the dispersion direction and  $0.8''/\text{pixel}$  in the spatial direction.

The data were flat fielded, masked for cosmic rays and bad pixels, and combined into a single spectrum for each galaxy. For most galaxies, sky subtraction was performed using the edges of the slit, though some used the sky exposures instead as described in Paper I. None of the galaxies in

this sample are large enough in angular size for light from the galaxy itself to significantly bias the sky measurement at the slit edges. The galaxy spectra were extracted in  $r_e/8$  apertures, with effective radii taken from Faber et al. (1989) where possible, and from de Vaucouleurs et al. (1995) otherwise (NGC 2534). Equivalent widths for the available Lick indices were calculated using a version of the `bwid` program, provided by R. M. Rich (Rich 1998). Velocity dispersion and emission corrections were performed using the standard methods described in Paper I. Emission corrections were non-negligible in all galaxies in this sample, as expected for objects with young stellar populations. Finally, the standard star observations detailed in Paper I were used to transform the index measurements onto the Lick/IDS system. Index errors were calculated using the error simulations and systematic uncertainties derived in Paper I. Measurements for all available indices are presented in Table 2.

### 3. Analysis

#### 3.1. Single Stellar Populations

One set of stellar population parameters was derived from the primary indices,  $H\beta$ ,  $Mgb$ ,  $Fe5270$ , and  $Fe5335$ . Models from Thomas, Maraston, & Bender (2003) were used to interpolate age,  $[Z/H]$ , and  $[\alpha/Fe]$  in the  $H\beta$ – $[MgFe]'$  (Fig. 6) and  $Mgb$ – $\langle Fe \rangle$  planes. The  $H\gamma$ – $[MgFe]'$  plane can also be used to interpolate stellar population parameters, using models designed for the higher-order Balmer lines by Thomas, Maraston, & Korn (2004) (Fig. 7). A discussion of the relative merits of the two Balmer lines as age indicators is presented in Paper I. Since the merger remnant sample suffers from considerable emission contamination, the ages derived using  $H\gamma$  as the age-sensitive index are expected to be more accurate than ages using  $H\beta$  as the age-sensitive index. Quoted uncertainties are derived from the index uncertainties in the manner described in Paper I; note that the resulting SSP uncertainties do not incorporate the systematic uncertainties associated with the choice of specific models and indices used to measure SSP quantities.

Ideally, SSP parameters should be measured using all available information, not just the handful of commonly-used indices described above. The multiple index fitting code of Proctor et al. (2004, hereafter P04) provides the most reliable measurements of age,  $[Z/H]$ , and  $[\alpha/Fe]$ , fitting the three SSP parameters simultaneously using every index measured from the galaxy spectrum. Of particular importance for the present sample, deviant indices such as Balmer lines with large emission corrections can be omitted from the fit. The drawback of this method is that it relies on a different calibration of  $[\alpha/Fe]$  than the Thomas et al. models. Both Thomas et al. and P04 take into account the variation of  $[\alpha/Fe]$  with  $[Fe/H]$  below solar metallicity in the stellar calibrators used in the construction of SSPs. P04 extends the correction to supersolar metallicities. This seemingly minor difference has major effects on correlations between SSP parameters. P04 showed that using the corrected calibration, the well-known  $[\alpha/Fe]$ – $\sigma$  relation is destroyed, while correlations between  $[\alpha/Fe]$  and age, and  $[\alpha/H]$  and  $\sigma$  are strengthened. An unfortunate consequence of the

calibration difference between P04 and other models is that the results of the multiple index fitting code cannot be directly compared to previous results.

The SSP parameters measured using all three methods are listed in Table 3; both the SSP values derived using  $H\gamma$  as the age-sensitive index and multi-index fitting values will be used in the subsequent analysis. Good fits were obtained for all galaxies using the latter method (Proctor 2005, private communication), though the fits for NGC 474 and NGC 1052 were noticeably worse than the rest.

Stellar population parameters age,  $[Z/H]$ , and  $[\alpha/Fe]$  are plotted against structural parameters  $\sigma$ ,  $M_B$ , and  $\log r_e$  in Fig. 8. Also shown are the galaxies from the volume limited sample described in Paper I and galaxies from the Gonzalez (1993, hereafter G93) sample not included in the volume-limited sample. Index measurements from G93 have been used to measure SSP parameters using the Thomas et al. (2003) models for consistency. The stellar population measurements from the latter samples are derived from  $H\beta$ – $[MgFe]'$  model grids. However, for the purpose of illustrating the underlying qualitative trends within a large and representative population of elliptical galaxies, the difference between SSP measurements using  $H\gamma$  or  $H\beta$  as the age-sensitive index is not of critical importance. Due to the difference in  $[\alpha/Fe]$  calibration, the results of the multi-index fitting are not as directly comparable. Figure 8 shows that the galaxies in the merger remnant sample have the same distribution of stellar population parameters as galaxies from the volume-limited sample with similar structural parameters. According to Kolmogorov-Smirnov tests, the probabilities that the samples are drawn from the same distribution are 0.997, 0.59, and 0.24 in age,  $[Z/H]$ , and  $[\alpha/Fe]$  respectively. With four of six galaxies (all six, using the multi-index fitting method) having SSP ages less than or equal to 6 Gyr, the merger remnant sample is, on average, significantly younger than the volume-limited sample as a whole. The young ages cannot be directly attributed to mergers, however, since these galaxies are on the low mass, faint, small radius end of the distribution of the volume-limited sample. The similarly young ages of galaxies in the volume-limited sample with comparable sizes and luminosities suggests downsizing (Cowie et al. 1996) as an adequate explanation.

The merger remnant sample is also plotted on the metallicity hyperplane in Fig. 9. This hyperplane was derived by (Trager et al. 2000) using principal component analysis in the four dimensional parameter space of velocity dispersion, age, metallicity, and  $[\alpha/Fe]$  abundance ratio. PC1 increases with  $\sigma$ ,  $[\alpha/Fe]$ , and to a lesser extent  $[Z/H]$ ; PC2 increases with age and decreases with  $[Z/H]$ ; and PC3 increases with  $[\alpha/Fe]$  and decreases with  $\sigma$ . Thus the remnants of major mergers, having low ages and  $[\alpha/Fe]$ , would be expected to have low values in each principal component. No galaxy in the merger remnant sample occupies that part of the hyperplane. The unusually low PC1 value of NGC 7332 is a result of a small velocity dispersion combined with low  $[\alpha/Fe]$ . The remaining galaxies in the sample are distributed similarly to the galaxies in the volume-limited sample. Note that the calibration difference between the multi-index fitting technique and previous SSP model estimates prevents any meaningful use of the multi-index fits in reference to the hyperplane. As mentioned previously, the  $[\alpha/Fe]$ – $\sigma$  relation (represented by the first principal

component in the Trager et al. (2000) hyperplane) disappears using the P04 calibration.

The distribution of the merger remnant sample along the  $Z$ -plane (Trager et al. 2000) is shown in Fig. 10. Note that as described in Paper I the best fit line must be offset slightly in  $[Z/H]$  to account for the use of different models than in Trager et al. (2000). Trager et al. (2000) argued that a scaling between age and metallicity can most sensibly be maintained over time by episodes of star formation within the host galaxy. Stellar populations formed in a single starburst cannot maintain a linear  $Z$ -plane projection in this space of  $[Z/H]$ ,  $\log t$ , and  $\log \sigma$  since  $\log t$  changes more rapidly at younger ages than at older ages. A major merger between two spiral galaxies should not obey this same relation barring an improbable conspiracy of stellar population parameters in the progenitor galaxies. The metallicity and abundance ratios of the stars formed in the merger starburst must have the proper scaling with respect to the existing stellar populations of the progenitor galaxies in order for the merger remnant to return to the  $Z$ -plane and the metallicity hyperplane. Further, the range of allowed metallicities for the starburst population is smaller for younger remnants than for older remnants. As with the hyperplane above, multi-index fits cannot be meaningfully plotted on the  $Z$ -plane.

NGC 2534 is the only outlier from the  $Z$ -plane defined by the galaxies in the volume-limited sample. The measured  $[Z/H]$  for this galaxy is too low by  $\sim 0.3$  dex for it to lie along the plane; alternatively an age older by  $\sim 3.5$  Gyr would bring NGC 2534 onto the  $Z$ -plane at the present  $[Z/H]$  value. The latter is the more physically plausible explanation: a small mass fraction starburst can easily decrease the SSP age measurement by that amount and shift a galaxy off of the  $Z$ -plane for several Gyr. Whether or not passive evolution ages the galaxy back to the  $Z$ -plane depends on the metallicities of the original and starburst populations (Trager et al. 2000). A major merger event could explain the location of NGC 2534 in this parameter space; this possibility will be discussed in detail in § 4. It is interesting that the other five galaxies all lie on the  $Z$ -plane in good agreement with the galaxies from Paper I and G93. Since the multi-index fits are not usable for this analysis, the errors for NGC 1052 are extremely large and it is not a significant outlier. As candidate merger remnants, these galaxies would also be expected to lie above this projection of the plane for the same reasons as NGC 2534. It is worth noting that although galaxies which lie above the  $Z$ -plane are likely to have a frosting population of young stars, not all galaxies with such a frosting population will necessarily lie above the  $Z$ -plane. However, gas originating in two distinct galaxies is unlikely to have the necessary scaling of metal abundances to return the resulting merger remnant to the  $Z$ -plane. The fact that so many suspected merger remnants — NGC 474, NGC 3619, NGC 5903, NGC 7332; NGC 3610 (Howell et al. 2004); NGC 584, NGC 1700, NGC 5831, NGC 6702 (Trager et al. 2000) — do lie along the  $Z$ -plane is therefore an intriguing mystery. Alternatively, this may indicate that the  $Z$ -plane is not as useful a discriminant between past star formation histories as it appears, since almost all ellipticals regardless of formation mechanism lie on this plane.

#### 4. Discussion and Conclusions

A small sample of merger remnant galaxies has been selected based primarily on evidence of HI tidal debris. High quality spectral line index measurements have been used to estimate stellar population parameters (age, metallicity,  $\alpha$ -enhancement) using the best available SSP models and multi-index fitting techniques.

Four galaxies, NGC 474, NGC 1052, NGC 3619, and NGC 5903, have broadly similar properties. All lie along the  $Z$ -plane as defined by the volume-limited sample of Paper I. All have intermediate SSP ages (4–6 Gyr) as measured using the multi-index fitting method of P04. These galaxies have stellar populations more consistent with the volume-limited sample (Paper I) than with predictions of recent major merger remnants. The stellar population measured for NGC 1052 can be compared with the definitive study of Pierce et al. (2005). The results of the multi-index fit are in reasonable agreement with Pierce et al. (2005), despite the fact that measurements relying on either Balmer line are extremely inaccurate due to the strong emission contamination.

The young SSP age and relatively low  $[Z/H]$  of NGC 2534 make it an outlier from the  $Z$ -plane in precisely the sense one would expect of a merger remnant with a small (by mass fraction) young population overlying an older population. However, the  $[\alpha/Fe]$  ratio in NGC 2534 is very large for an object in which most of the stars formed in spiral galaxies, or from gas enriched with iron by the long continuous star formation typical of spirals. Taking into account the relatively small velocity dispersion, NGC 2534 is somewhat *more*  $\alpha$ -enhanced than most elliptical galaxies (Fig. 8). This high  $[\alpha/Fe]$  ratio places the galaxy at a very high PC3 value in the metallicity hyperplane. Instead of the remnant of a major merger, these results are more consistent with NGC 2534 being an old, pre-existing elliptical which recently accreted a small, gas-rich companion.

NGC 7332 is another good match to merger remnant expectations. The SSP measurements for NGC 7332 are in excellent agreement with other studies (Falc3n-Barroso et al. 2004; Terlevich & Forbes 2002) when the  $H\gamma$  model grids are used. The multi-index fit presented here yields a significantly younger age and higher metallicity. The extreme position of NGC 7332 in Fig. 9 is due to the combination of low velocity dispersion and low (near solar)  $[\alpha/Fe]$ . The measurement of  $[\alpha/Fe] = +0.15$  (multi-index fit) is somewhat larger than predicted (Thomas et al. 1999), and is also consistent with galaxies of similar size in the volume-limited sample. As discussed above and in Trager et al. (2000), the metallicities of the progenitor galaxies would have to be carefully matched for the merger remnant to lie along the  $Z$ -plane as NGC 7332 does.

Fundamental Plane residuals provide an independent indication of anomalously young ages such as would be produced by a merger-induced starburst (Forbes, Ponman, & Brown 1998). The study of Rothberg & Joseph (2005) showed that optically selected merger remnants which deviate from the Fundamental Plane do so only in having higher surface brightness. Prugniel & Simien (1996) calculated Fundamental Plane residuals for five galaxies in the present sample. The residual for NGC 2534 was calculated using Equation 4 of Prugniel & Simien (1996) with data taken from de Vaucouleurs et al. (1995). The Fundamental Plane residuals of NGC 474, 1052, 2534, 3619,

and 5903 range from +0.03 to +0.11. Only NGC 7332 has a large negative residual indicative of a young age (Forbes, Ponman, & Brown 1998).

To summarize, two of the six galaxies fit some of the expected properties of a “King gap” merger remnant (Thomas et al. 1999), though neither galaxy precisely fits every prediction. The positions of NGC 7332 on the hyper-plane and relative to the Fundamental Plane suggest that it is the most likely merger remnant in the sample, though the abundance ratio  $[\alpha/\text{Fe}]$  (multi-index fit) and position on the  $Z$ -plane remain difficult to explain. Taken as a group the SSP properties of the merger remnant sample are not substantially different from those of structurally similar (in velocity dispersion, luminosity, or radius) galaxies from the volume-limited sample of Paper I (Fig. 8). The merger remnant sample is consistent with being drawn from the same distribution as the volume-limited sample in each SSP parameter.

The disagreement between derived SSP quantities and merger remnant predictions should not necessarily be taken to imply that the galaxies are not merger remnants. The similarities between the properties of the merger remnant sample and the volume-limited sample, as well as the non-detection of the expected major merger signatures (low age combined with near solar  $[\alpha/\text{Fe}]$ ) in four of the six galaxies suggest that this “merger remnant” sample may include few remnants of recent major mergers. Instead, as proposed for NGC 2534, these galaxies are more consistent with being older elliptical galaxies which recently accreted a gas-rich companion galaxy. It is also possible that the predictions for the stellar populations of major merger remnants are not applicable to the galaxies in this sample. Thomas et al. (1999) consider a merger of two galaxies similar to the Milky Way; more gas-rich progenitors and thus a larger starburst by mass fraction would result in supersolar  $[\alpha/\text{Fe}]$ . A top-heavy IMF has long been suggested as another explanation for the large observed values of  $[\alpha/\text{Fe}]$  in early-type galaxies. Nagashima et al. (2005) incorporated such an IMF into semi-analytical hierarchical galaxy formation models which reproduce the observed  $[\alpha/\text{Fe}]$  values for some elliptical galaxies, though the models at present fail to reproduce the  $[\alpha/\text{Fe}]$ - $\sigma$  relation. As P04 discussed extensively, the calibration of  $[\alpha/\text{Fe}]$  is tremendously important since many galaxy formation models use the  $[\alpha/\text{Fe}]$ - $\sigma$  relation as a constraint.

This research has made use of the NASA/IPAC Extragalactic Database (NED) which is operated by the Jet Propulsion Laboratory, California Institute of Technology, under contract with the National Aeronautics and Space Administration. This work also made use of the Gauss-Hermite Pixel Fitting Software developed by R.P. van der Marel. J. H. H. was supported in part by an ARCS Fellowship. This research was supported in part by NSF grant AST-0507483 to the University of California Santa Cruz. We thank Ricardo Schiavon, Sandy Faber, Jean Brodie, and Mike Beasley for helpful conversations, Rob Proctor for the use of his multi-index fitting code and several important comments, and the anonymous referee for comments which significantly improved the paper.



## REFERENCES

- Appleton, P. N., Pedlar, A., & Wilkinson, A. 1990, *ApJ*, 357, 426
- Ashman, K. M. & Zepf, S. E. 1992, *ApJ*, 384, 50
- Burstein, D., Krumm, N., & Salpeter, E. E. 1987, *AJ*, 94, 883
- Cowie, L. L., Songaila, A., Hu, E. M., & Cohen, J. G. 1996, *AJ*, 112, 839
- de Vaucouleurs, G., de Vaucouleurs, A., Corwin, H. G., Buta, R. J., Paturel, G., & Fouque, P. 1995, *VizieR Online Data Catalog*, 7155, 0
- Faber, S. M., Wegner, G., Burstein, D., Davies, R. L., Dressler, A., Lynden-Bell, D., & Terlevich, R. J. 1989, *ApJS*, 69, 763
- Falcón-Barroso, J., et al. 2004, *MNRAS*, 350, 35
- Forbes, D. A., Ponman, T. J., & Brown, R. J. N. 1998, *ApJ*, 508, L43
- Gonzalez, J. J. 1993, Ph.D. thesis, University of California, Santa Cruz (G93)
- Heckman, T. M. 1980, *A&A*, 87, 152
- Hibbard, J. E. & Mihos, J. C. 1995, *AJ*, 110, 140
- Hibbard, J. E. & Sansom, A. E. 2003, *AJ*, 125, 667
- Howell, J. H. 2005, *AJ*, accepted (Paper I)
- Howell, J. H., Brodie, J. P., Strader, J., Forbes, D. A., & Proctor, R. 2004, *AJ*, 128, 2749
- Kauffmann, G. 1996, *MNRAS*, 281, 487
- Kaviraj, S., Devriendt, J. E. G., Ferreras, I., & Yi, S. K. 2005, *MNRAS*, 360, 60
- King, I. R. 1977, in *The Evolution of Galaxies and Stellar Populations*, edited by B. M. Tinsley and R. B. Larson (Yale University Observatory, New Haven), p. 418
- Larson, R. B. 1974, *MNRAS*, 166, 585
- Nagashima, M., Lacey, C. G., Okamoto, T., Baugh, C. M., Frenk, C. S., & Cole, S. 2005, *MNRAS*, L72
- Pierce, M., Brodie, J. P., Forbes, D. A., Beasley, M. A., Proctor, R., & Strader, J. 2005, *MNRAS*, 358, 419
- Proctor, R. N., Forbes, D. A., Hau, G. K. T., Beasley, M. A., De Silva, G. M., Contreras, R., & Terlevich, A. I. 2004, *MNRAS*, 349, 1381 (P04)

- Prugniel, P. & Simien, F. 1996, *A&A*, 309, 749
- Rich, R. M. 1998, ASP Conf. Ser. 147, *Abundance Profiles: Diagnostic Tools for Galaxy History*, ed. D. Friedli, M. Edmunds, C. Robert, & L. Drissen (San Francisco: ASP), p. 36
- Rothberg, B., & Joseph, R. D., astro-ph/0510019
- Schiminovich, D., van Gorkom, J. H., Dijkstra, M., Li, Y., Petric, A., & van der Hulst, J. M. 2001, ASP Conf. Ser. 240: *Gas and Galaxy Evolution*, 864
- Schweizer, F. & Seitzer, P. 1992, *AJ*, 104, 1039
- Terlevich, A. I. & Forbes, D. A. 2002, *MNRAS*, 330, 547
- Thomas, D. 1999, *MNRAS*, 306, 655
- Thomas, D., Greggio, L., & Bender, R. 1999, *MNRAS*, 302, 537
- Thomas, D., Maraston, C., & Bender, R. 2003, *MNRAS*, 339, 897
- Thomas, D., Maraston, C., & Korn, A. 2004, *MNRAS*, 351, L19
- Toomre, A. & Toomre, J. 1972, *ApJ*, 178, 623
- Trager, S. C., Faber, S. M., Worthey, G., & Gonzalez, J. J. 2000b, *AJ*, 120, 165
- van Driel, W., Balkowski, C., & van Woerden, H. 1989, *A&A*, 218, 49
- van Gorkom, J. H., Knapp, G. R., Raimond, E., Faber, S. M., & Gallagher, J. S. 1986, *AJ*, 91, 791
- Worthey, G. 1994, *ApJS*, 95, 107

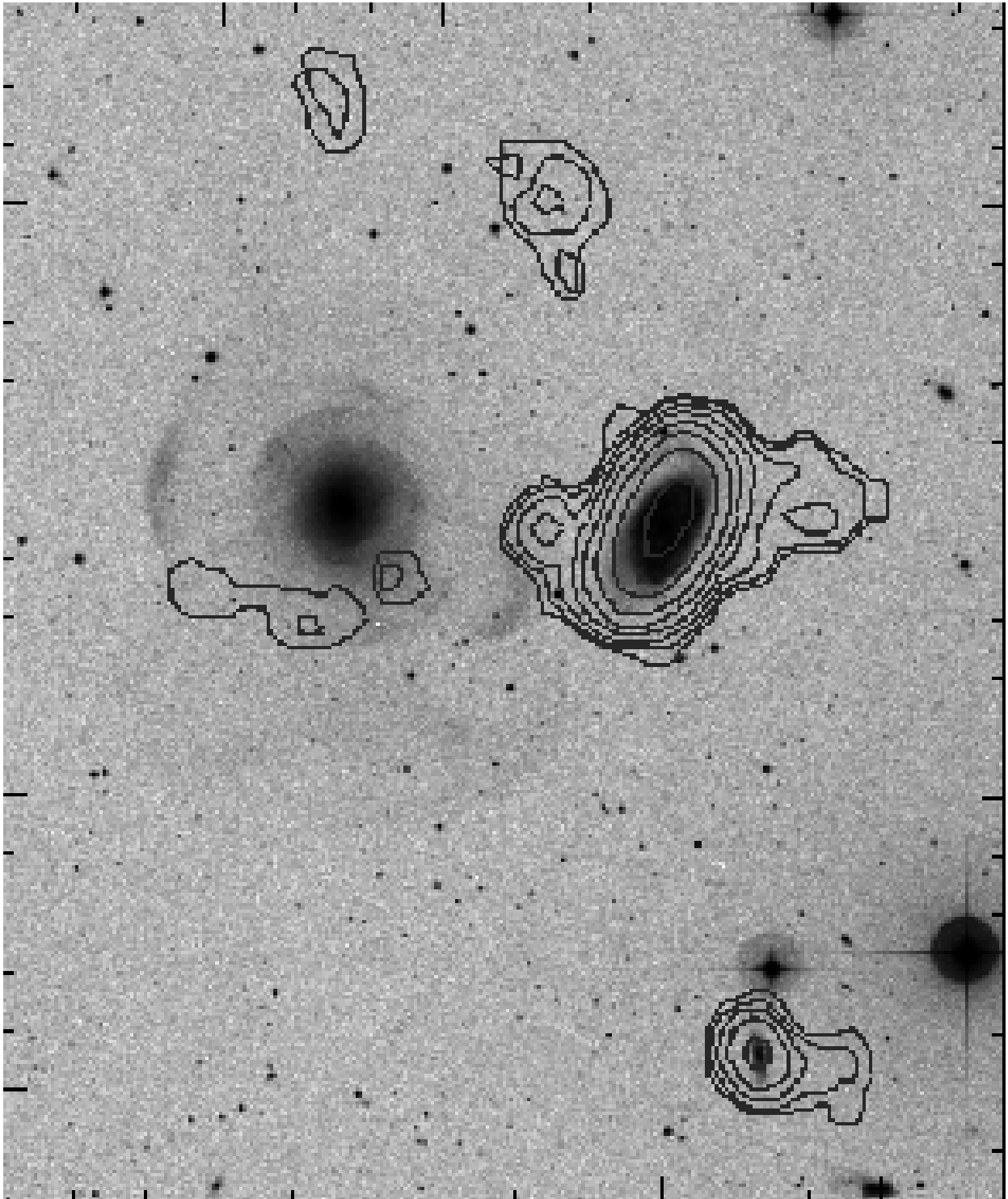


Fig. 1.— Contours of HI emission are overlaid on the DSS image of NGC 474 (left) and the nearby spiral galaxy NGC 470 (right). The disturbed, shell galaxy morphology of NGC 474 is clearly evident. Although NGC 474 has little or no HI of its own, it appears to have accreted gas from NGC 470. This figure originally appeared in Schiminovich et al. (2001).

Table 2. Index Measurements:  $r_e/8$  Aperture

Galaxy	$\sigma$	Ca4227	G4300	H $\gamma_F$	Fe4383	Ca4455	Fe4531	C4668	H $\beta$	[OIII] $\lambda$ 5007	Fe5015	Mgb	Fe5270	Fe5335	Fe5406	[MgFe]'
NGC 474	169	1.12	4.75	-1.05	5.34	1.58	3.75	6.79	1.86	-0.49	6.12	4.55	3.25	2.55	1.56	3.73
	4	0.10	0.14	0.11	0.09	0.05	0.11	0.12	0.07	0.07	0.20	0.05	0.06	0.09	0.09	0.05
NGC 1052	215	1.20	5.72	-2.17	6.50	1.43	3.78	8.24	1.21	-3.71	1.90	5.96	3.05	2.78	1.88	4.21
	4	0.10	0.14	0.38	0.09	0.05	0.11	0.12	0.7	1.0	0.64	0.05	0.06	0.09	0.09	0.05
NGC 2534	158	0.91	4.25	0.01	3.90	1.17	3.24	6.12	2.27	-1.02	4.74	3.70	2.56	2.12	1.50	3.00
	6	0.10	0.14	0.13	0.21	0.14	0.09	0.20	0.11	0.14	0.29	0.06	0.09	0.13	0.09	0.07
NGC 3619	179	1.08	5.56	-1.33	5.81	1.43	3.88	7.48	2.25	-1.25	4.63	4.47	3.19	2.99	1.96	3.74
	4	0.10	0.16	0.10	0.18	0.07	0.07	0.19	0.12	0.16	0.14	0.06	0.09	0.13	0.09	0.07
NGC 5903	211	1.40	5.97	-2.10	5.73	1.73	3.72	7.00	1.92	-0.42	5.83	4.57	3.05	2.78	1.63	3.69
	4	0.10	0.16	0.08	0.18	0.07	0.07	0.19	0.08	0.08	0.12	0.06	0.09	0.13	0.09	0.07
NGC 7332	128	1.14	5.14	-1.07	4.66	1.56	3.74	7.43	2.47	-0.32	6.09	3.83	3.13	2.84	1.87	3.42
	4	0.10	0.14	0.13	0.21	0.14	0.09	0.20	0.09	0.10	0.29	0.05	0.06	0.09	0.09	0.05

Table 3. Stellar Population Parameters

Galaxy	$\sigma$ km/s	$\sigma_\sigma$	Method	Age Gyr	$\sigma_t$	[Z/H] dex	$\sigma_Z$	[ $\alpha$ /Fe] dex	$\sigma_\alpha$
NGC 474	169	4	H $\beta$ grid	3.4	0.6	0.55	0.09	0.27	0.04
			H $\gamma$ grid	3.45	0.8	0.53	0.07	0.27	0.04
			Multi-index fit	4.4	1.2	0.38	0.07	0.24	0.03
NGC 1052	215	5	H $\beta$ grid	16	14	0.42	0.3	0.44	0.12
			H $\gamma$ grid	10.9	8	0.48	0.16	0.46	0.09
			Multi-index fit	4	2	0.45	0.08	0.21	0.05
NGC 2534	158	6	H $\beta$ grid	2.2	0.9	0.23	0.08	0.33	0.07
			H $\gamma$ grid	2.8	0.7	0.17	0.06	0.30	0.07
			Multi-index fit	2.7	0.2	0.20	0.05	0.27	0.04
NGC 3619	179	4	H $\beta$ grid	1.2	1	0.94	0.16	0.33	0.05
			H $\gamma$ grid	5.4	1.5	0.43	0.06	0.18	0.05
			Multi-index fit	4.0	0.8	0.43	0.06	0.15	0.03
NGC 5903	211	4	H $\beta$ grid	3.0	0.5	0.58	0.09	0.28	0.04
			H $\gamma$ grid	17.5	2	0.16	0.1	0.18	0.04
			Multi-index fit	6.0	1.6	0.28	0.04	0.15	0.05
NGC 7332	128	4	H $\beta$ grid	0.8	0.3	0.88	0.14	0.26	0.04
			H $\gamma$ grid	6.1	1	0.22	0.06	0.06	0.04
			Multi-index fit	1.8	0.2	0.58	0.09	0.15	0.03

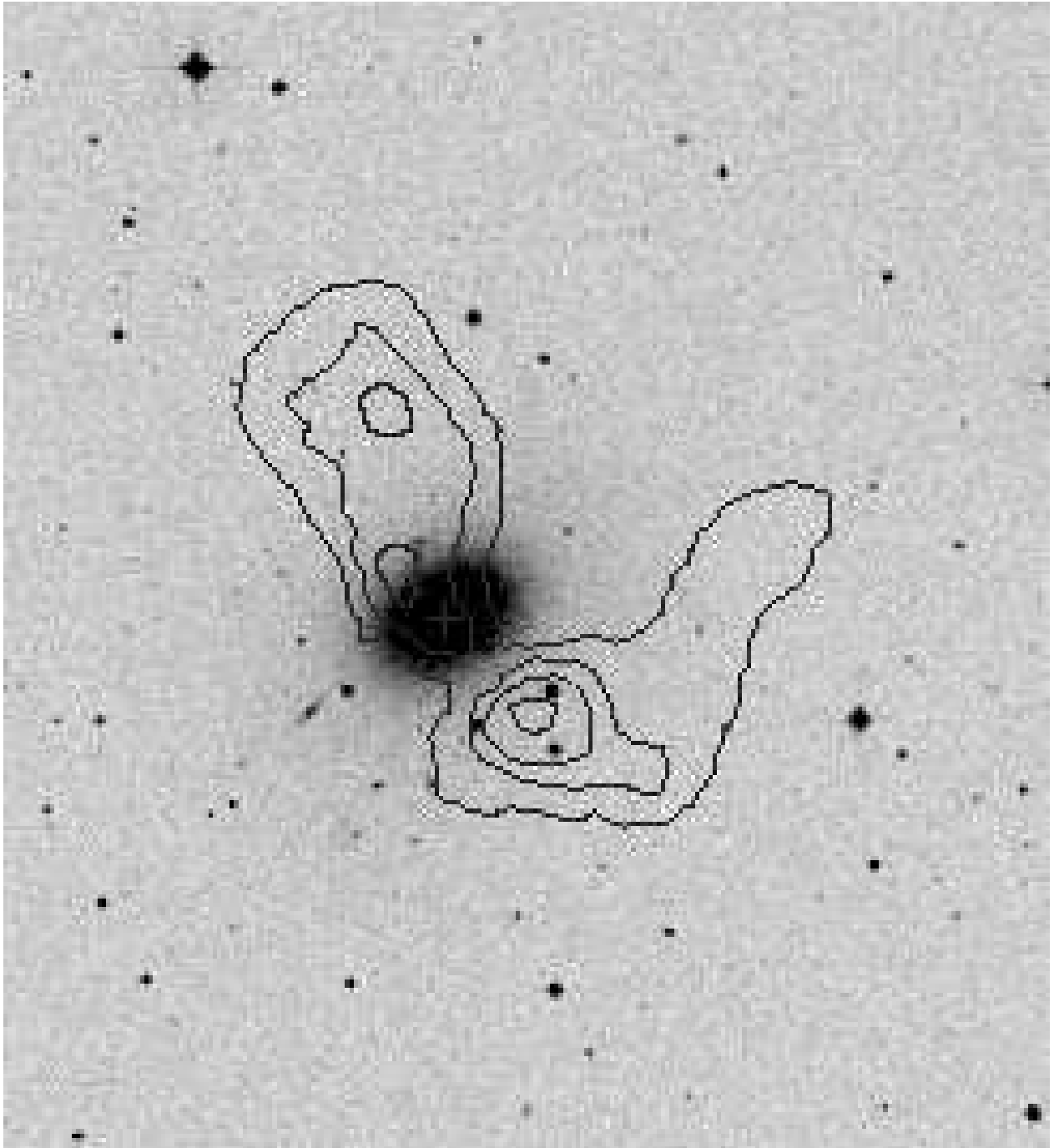


Fig. 2.— Contours of HI emission are overlaid on the DSS image of NGC 1052. This figure originally appeared in van Gorkom et al. (1986).

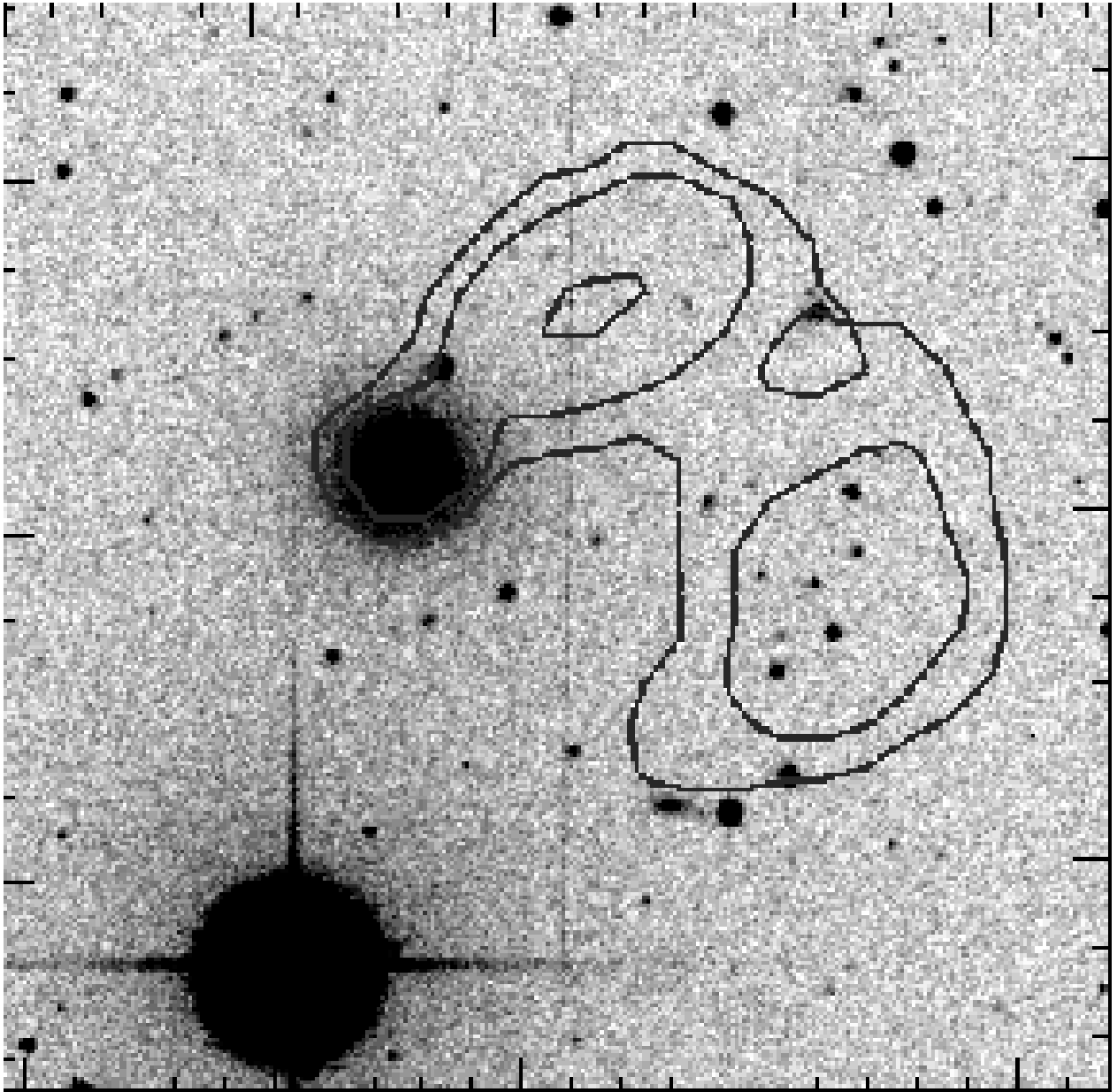


Fig. 3.— Contours of HI emission are overlaid on the DSS image of NGC 2534. This figure originally appeared in Schiminovich et al. (2001).

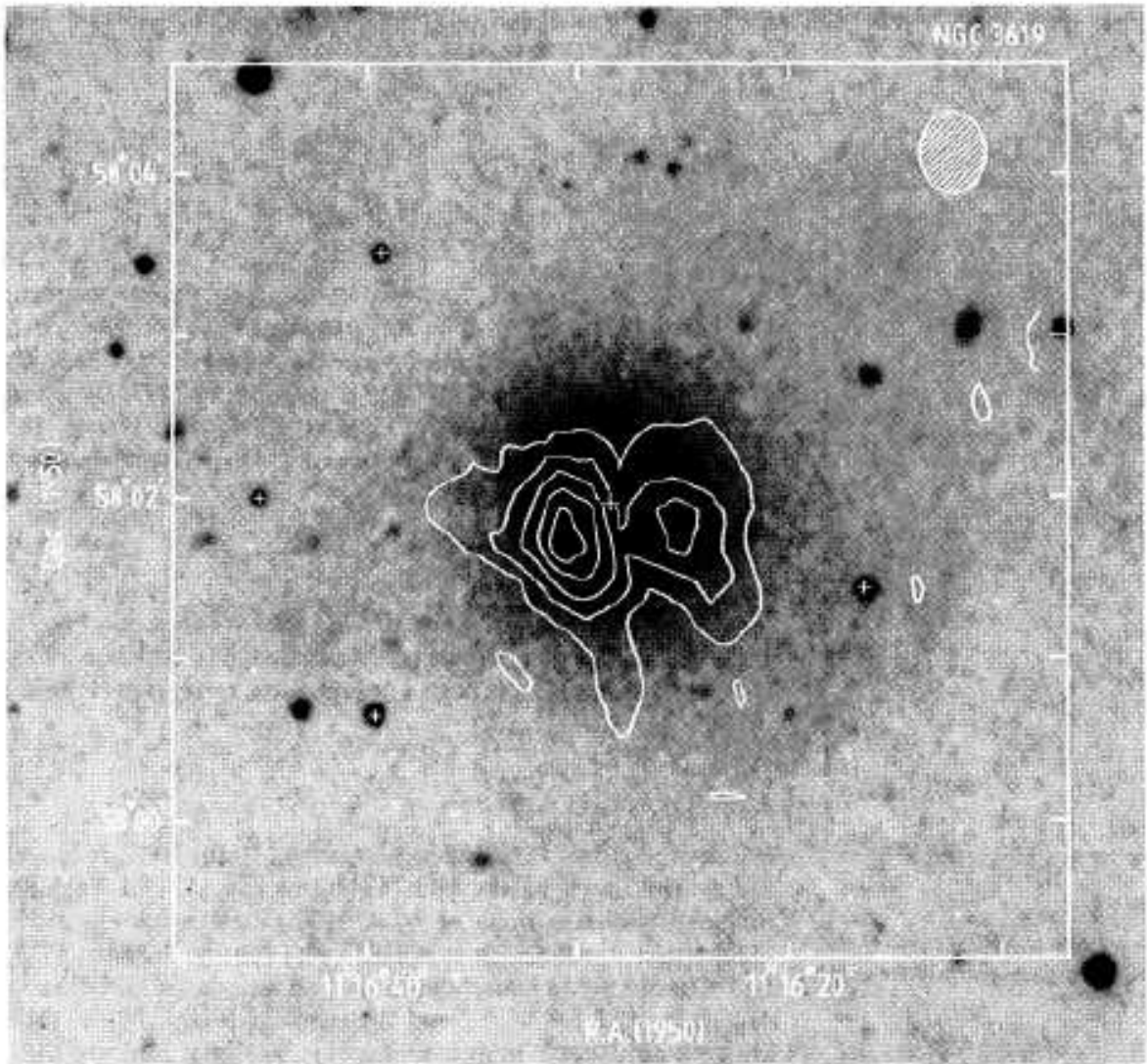


Fig. 4.— Contours of HI emission are overlaid on the DSS image of NGC 3619. This figure originally appeared in van Driel, Balkowski, & van Woerden (1989).



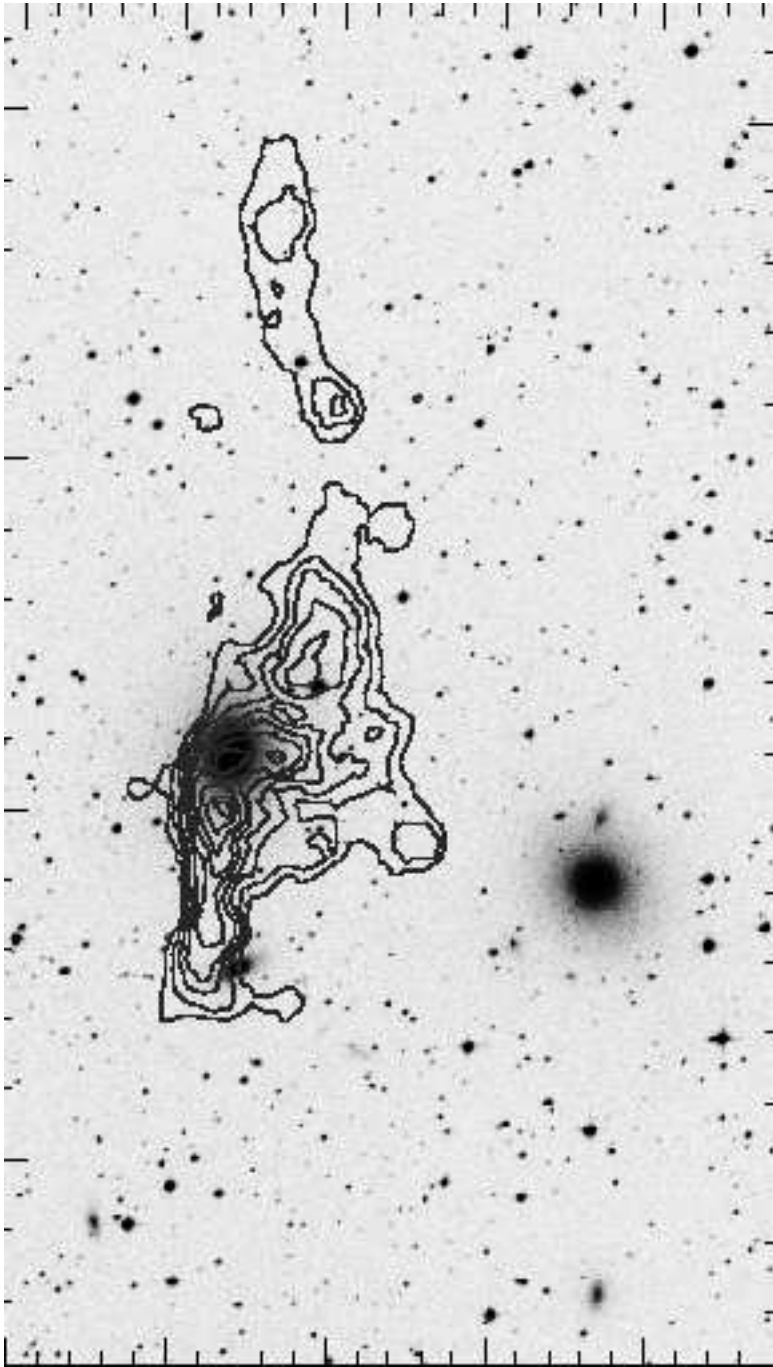


Fig. 5.— Contours of HI emission are overlaid on the DSS image of NGC 5903. This figure originally appeared in Appleton, Pedlar, & Wilkinson (1990).

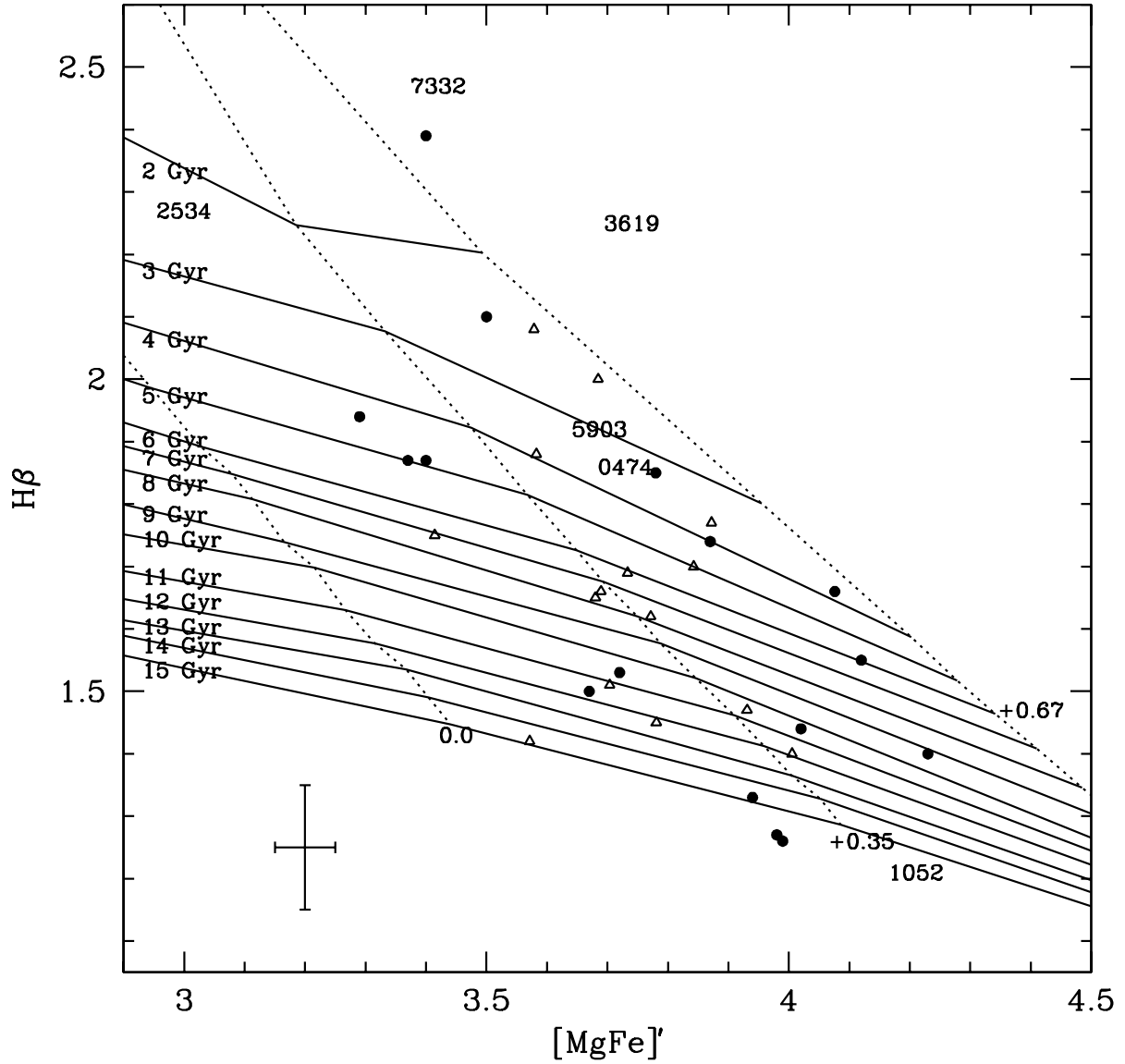


Fig. 6.— Galaxies from the merger remnant sample are plotted on the  $H\beta$  vs.  $[MgFe]'$  plane (NGC numbers). Also shown are galaxies from the volume limited sample. Solid circles are from Paper I; open triangles are from G93. Models are from Thomas et al. (2003). Typical error bars are in the lower left.

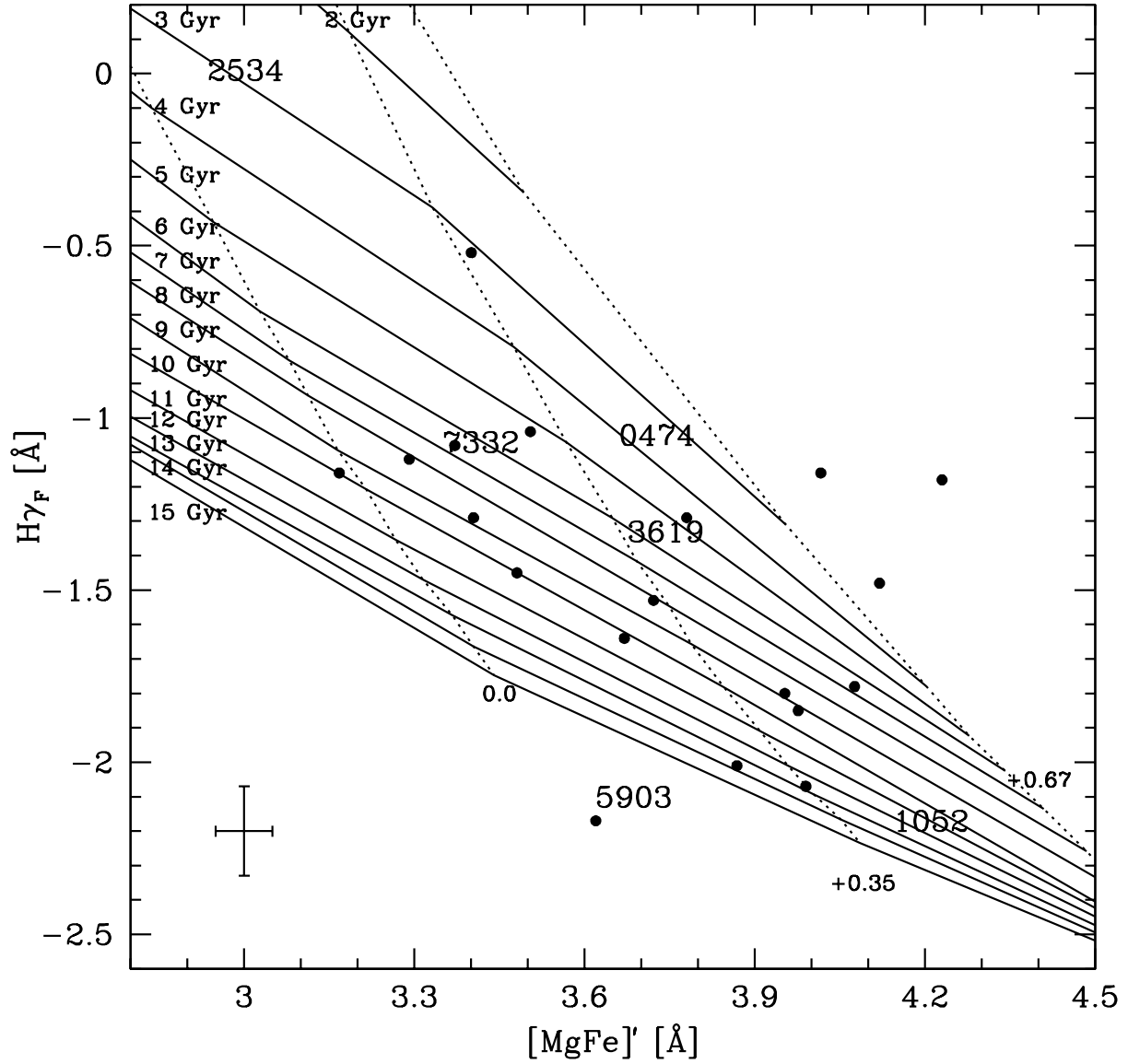


Fig. 7.— Galaxies from the merger remnant sample are plotted on the  $H\gamma_F$  vs.  $[MgFe]'$  plane (NGC numbers). Also shown are galaxies from the volume limited sample (black points; Paper I). Models are from Thomas et al. (2004). Typical error bars are in the lower left.

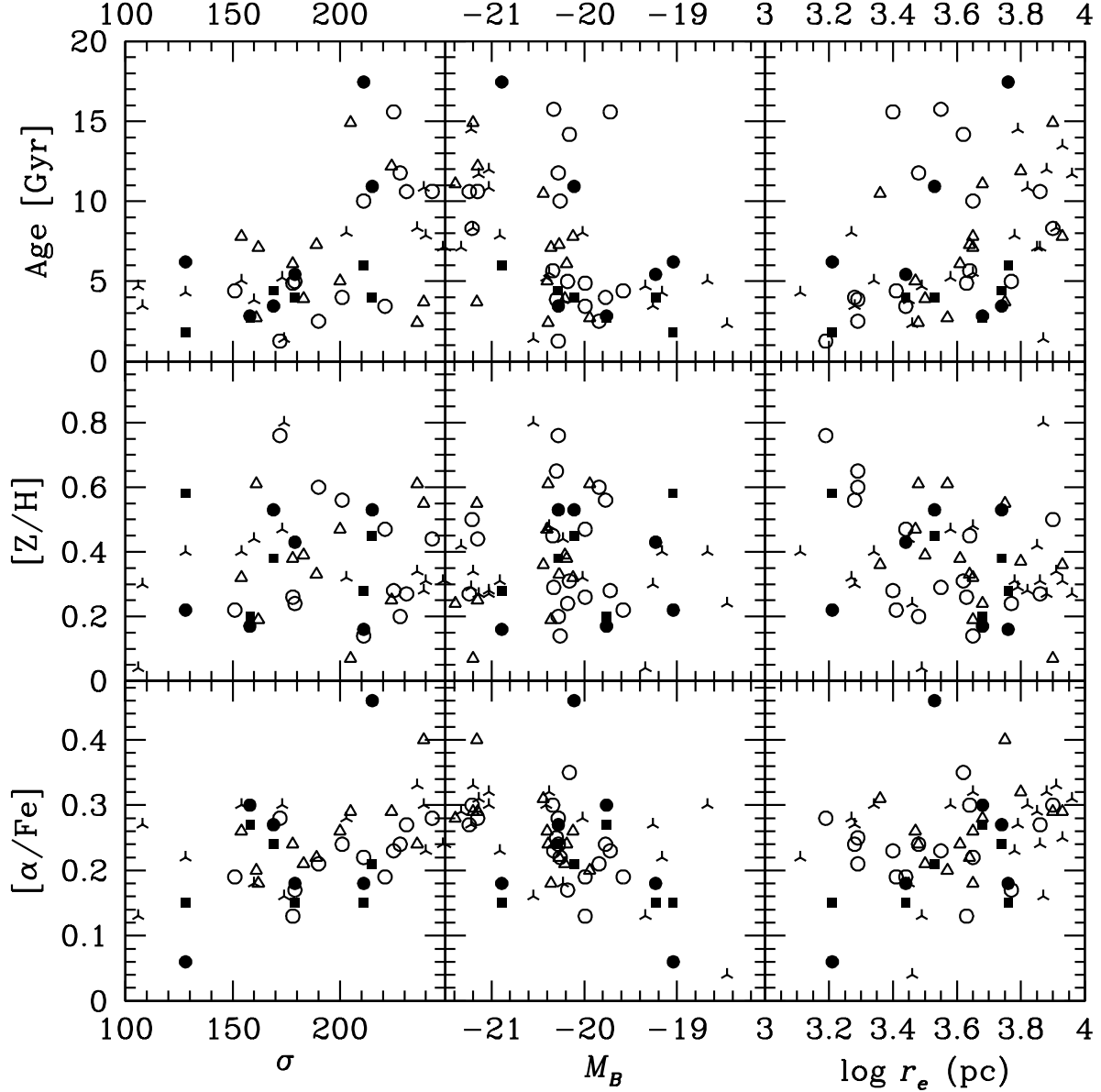


Fig. 8.— Comparison between parameters relating to the average stellar composition (age,  $[Z/H]$ ,  $[\alpha/Fe]$ ) and parameters relating to galaxy size ( $\sigma$ ,  $M_B$ ,  $\log r_e$ ). Open circles are galaxies from the volume-limited sample (Paper I), open triangles are G93 galaxies included in the volume-limited sample, and three-pointed stars are the G93 galaxies not included in the volume-limited sample. The solid circles represent the merger remnant sample as measured using the  $H\gamma$  index SSP models, while the solid squares are the same galaxies as measured by the multi-index fitting procedure. Contrary to expectations (Thomas et al. 1999), the merger remnant sample is distributed consistently with the volume-limited sample.

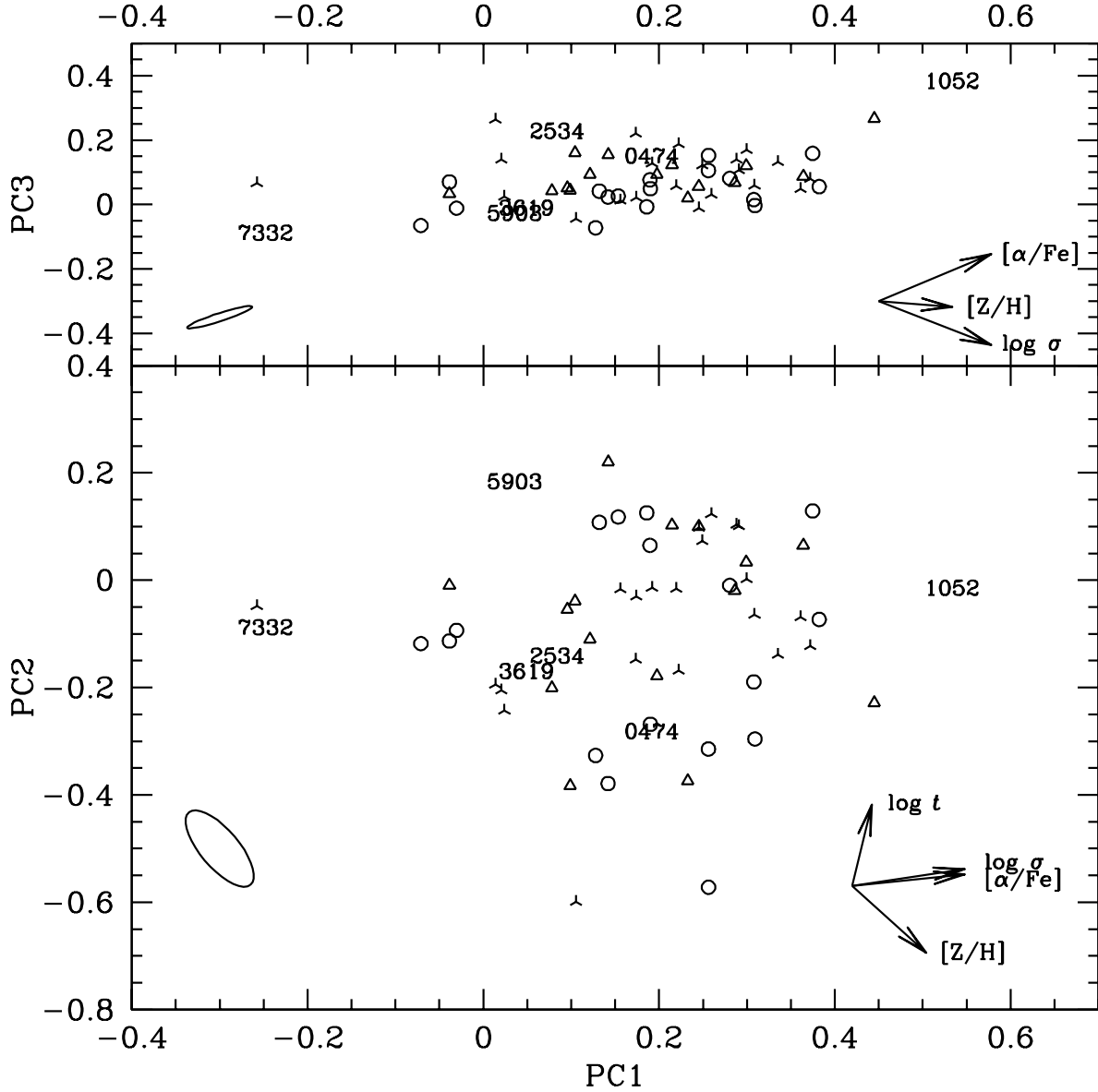


Fig. 9.— Merger remnant galaxies plotted on the metallicity hyperplane. Open symbols and three-pointed stars are as in Fig. 8. Merger remnant galaxies are plotted using their NGC numbers. Projections of each SSP parameter along principal component axes are shown in the lower right. PC1 depends primarily on velocity dispersion and  $\alpha$ -enhancement, PC2 depends primarily on age and metallicity, and PC3 measures deviations from the  $[\alpha/\text{Fe}]-\sigma$  relation. See Paper I for details. The merger remnant galaxies are generally consistent with the distribution of the volume-limited sample. NGC 7332 has the low PC1 value expected of a merger remnant (Thomas et al. 1999); however the galaxy is otherwise consistent with the volume-limited sample.

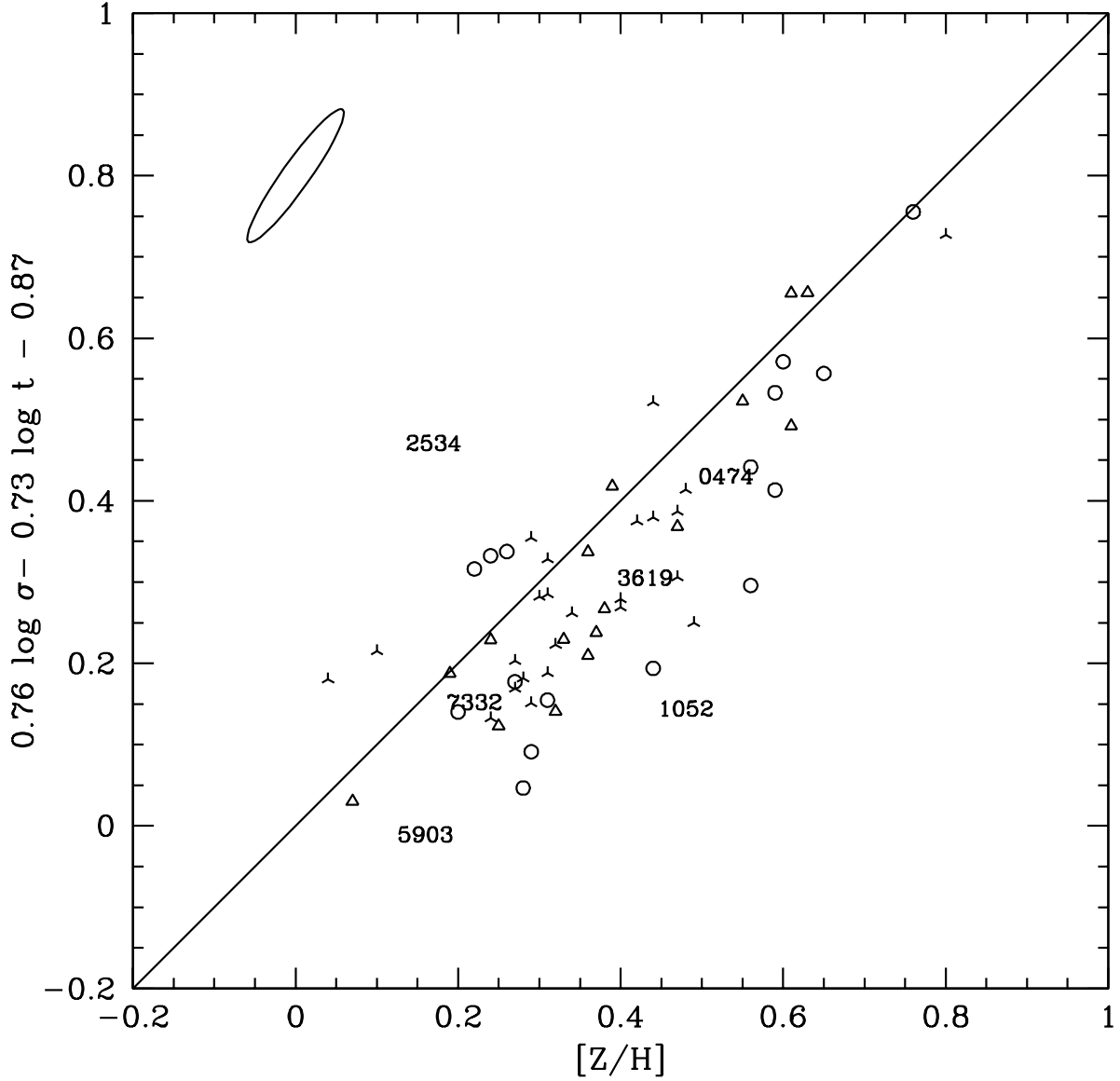


Fig. 10.— Merger remnant galaxies plotted on the  $Z$ -plane. Points are as in Fig. 9. The best-fit line from Trager et al. (2000) is shown. The offset between this line and the locus of the volume-limited sample is due to differences in models between this work and Trager et al. (2000); see text for details. The deviation of NGC 2534 from the plane is plausibly explained by a recent starburst overlying an older stellar population that constitutes the majority of the galaxy’s stellar mass.